Available online at www.sciencedirect.com

ScienceDirect

Procedia Manufacturing 29 (2019) 464–471

Procedia MANUFACTURING

www.elsevier.com/locate/procedia

18th International Conference on Sheet Metal, SHEMET 2019

Approach for modelling the Taylor-Quinney coefficient of high strength steels

Bernd-Arno Behrens, Alexander Chugreev, Florian Bohne, Ralf Lorenz*

Institute of Forming Technology and Machines, Leibniz University Hannover, 30823 Garbsen, Germany

Abstract

Precise knowledge of the temperature that arises in the material during plastic forming is of crucial importance, as it has a significant influence on material behaviour and therefore on the forming process. In order to describe the amount of heat that is generated during plastic forming accurately, the Taylor-Quinney coefficient β was introduced as the ratio of dissipated heat to plastic work and generally assumed to be a constant value. However, recent studies have shown that there is a dependency on material and process-specific parameters. In this study, the Taylor-Quinney coefficient β is shown as a function of strain and being influenced by the test specific strain rate and stress state. The tested material is a dual-phase steel HCT980X. The uniaxial tensile test and the Marciniak test with different tallied specimen at forming-relevant global strain rates were investigated. By means of thermographic and optical measuring systems the temperature and local strains were recorded during the tests. Based on an approach similar to the finite volume method, both experimental setups were modelled taking heat transfer effects into account. As a result, the Taylor-Quinney coefficient is calculated by means of experimental data. It is shown that the Taylor-Quinney coefficient is a variable value depending on the flow behaviour of the steel. The local strain rate and the specimen geometries of Marciniak test have a significant influence on the arising heat conduction. The stress state, however, has minor influence on β.

Keywords: Heat dissipation; Temperature; Heat transfer process; Taylor-Quinney coefficient

* Corresponding author. Tel.: +49-511-762-2329; fax: +49-511-762-3007.
E-mail address: lorenz@ifum.uni-hannover.de

10.1016/j.promfg.2019.02.163

1. Introduction

In the field of automotive body production, high-strength steels are commonly used because of their lightweight potential. Due to the high flow stresses and good formability, plastic work has a strong influence on the heat generation. During a cold forming process, a substantial fraction of the plastic work is converted into heat. In thermo-mechanic studies of Taylor, Farren and Quinney [1, 2] in 1925 and 1934, the measurements of heat in the centre of specimen during various deformation tests like torsion and compression of steels were published for the first time. They observed that only a small part of the plastic work is stored as internal energy due to cold working, the remaining energy input is dissipated into heat. Based on these results, the Taylor-Quinney coefficient was introduced as the ratio of thermal dissipation to plastic work (integral format β_{int}) or as the ratio of thermal rate of dissipation $\dot{Q}$ to plastic power $\dot{W}_{pl}$ (differential format β_{diff}). The plastic work $\dot{W}_{pl}$ can be calculated from the scalar product of the Cauchy stress tensor $\boldsymbol{\sigma}$ and the plastic rate of deformation tensor $\boldsymbol{d^{pl}}$.

$$\dot{W}_{pl} = \boldsymbol{\sigma} \circ \boldsymbol{d}^{pl} \tag{1.1}$$

In case of modelling the plastic yielding with help of the von-Mises yield criterion this can be expressed with help of the effective plastic strain rate ($\dot{\varphi}$) and the equivalent von Mises stress $\bar{\sigma}$ [3]:

$$\dot{W}_{pl} = \bar{\sigma}(\boldsymbol{\sigma})\dot{\varphi} \tag{1.2}$$

In case of adiabatic conditions the following definitions apply to the calculation of the Taylor-Quinney coefficient:

$$\beta_{int} = \frac{Q}{W_{pl}} = \frac{m \cdot c_p \cdot \Delta T}{W_{pl}} \tag{1.3}$$

$$\beta_{diff} = \frac{\dot{Q}}{\dot{W}_{pl}} = \frac{m \cdot c_p \cdot \dot{T}}{\dot{W}_{pl}} \tag{1.4}$$

In general, the Taylor-Quinney coefficient is assumed to have a constant value of 0.9. Further investigations have shown that the Taylor-Quinney coefficient of steels depends strongly on strain and strain rate. The focus of the measurements was either on the temperature or on the stored energy, which is generated by the forming process. Mainly infrared radiometry, infrared camera or thermocouples have been used in order to measure the temperature during the experimental tests [4, 5, 6].

In [7] Knysh et al. observed that the fraction of plastic work converted into heat is strain rate sensitive for two stainless steels. At low strains, β_{int} increases slightly with increasing strain rate. As transformation progresses, the behavior reverses. Fekete et al. [8] and Rittel et al. [9] quantified the influence of compression and tension on the Taylor-Quinney coefficient for different steels and alloys under dynamic load conditions. A large variation of β was observed. The resulting value for compression was significantly lower than the value for tension. However, due to the friction during compression, the results were inaccurate. For dual-phase steels Behrens et al. [10] identified that β_{int} is varying in the manner of functional dependence on strain and material from β_{int} = 1 at φ = 0.01 to β = 0.45 at φ = 0.18 for DP600 and from β_{int} = 0.69 at φ = 0.01 to β_{int} = 0.47 at φ = 0.18 for DP1000. This assumption was verified by means of numerical simulation of the performed tensile test.

With regard to the optimisation of forming processes and component design using FE simulation, a precise prediction of the temperature field in the component is required [11]. At the moment, there is no adequate material model that is capable of accurately reproducing the heat dissipation. In this paper, a new approach is chosen in order to calculate the Taylor-Quinney coefficient as a function of effective plastic strain. Furthermore, it is shown that process specific strain rates as well as stress states influence this function.

2. Materials and experimental methods

2.1. Materials

HCT980X steel has been investigated with a sheet thickness of 1.2 mm. An overview of the chemical composition is shown in Table 1. The dual-phase steel HCT980X is mainly used for the production of complex high-strength structural elements. Its structure consists mostly of a soft ferritic matrix with hard martensite inclusions. The martensite provides a considerable increase in strength. In order to improve formability, fractions of retained austenite and bainite may be contained in the microstructure.

Table 1. Chemical composition of the steel samples in wt %.

Steel grade	C	Si	Mn	P	S	Al	Ti + Nb	Cr + Mo	V	B
HCT980X	0.15	0.69	1.85	0.017	0.0003	0.031	0.11	0.34	0.004	0.0004

For calculating the plastic work done with respect to equation (1.3), flow curves have been determined experimentally at room temperature. In the tensile test, only true stress values up to the beginning of the necking can be recorded accurately. Therefore, the experimental results were approximated by means of different model approaches to consider advanced plastic work behaviour. For HCT980X, the approach which accurately reproduces the flow behaviour based on the experimental results, is a combination of 60 % Swift [12] and 40 % Voce [13].

$$k_{f,Swift} = a_1 \cdot (b_1 + \varphi)^{c_1} \tag{2.1}$$

$$k_{f,Voce} = b_2 - (b_2 - a_2) \cdot e^{-c_2 \cdot \varphi} \tag{2.2}$$

$$k_{f,comb} = \gamma \cdot k_{f,Swift} + (1 - \gamma) \cdot k_{f,Voce} \tag{2.3}$$

Where $k_{f,Swift}$ and $k_{f,Voce}$ correspond to the true stresses according to the respective approach, $k_{f,comb}$ to the combined true stress, φ to the effective plastic strain and a_i, b_i, c_i $(i = \{1; 2\})$ to the derived material-specific parameters that are presented in Table 2. The calculated correlation coefficient for the combined flow curve model is 0.991.

Table 2. Material-specific parameters for the flow curve terms

a_1	a_2	b_1	b_2	c_1	c_2	γ
1427	794.5	2.43e-14	1302	0.09833	13.76	0.6

2.2. Tensile test

The tensile tests according to DIN EN ISO 6892-1 [14] were carried out on the S100/ZD Dynamess machine for strain rates of $0.01\ s^{-1}$ and $0.1\ s^{-1}$. The ARAMIS optical measuring system (GOM GmbH) was used for recording the surface strains with a frequency of 10 frames per second using digital image correlation (DIC). In order to estimate the internal energy, the temperature was recorded by means of an IR (infrared) camera (FLIR A35). The FLIR camera system is able to record 60 frames per second with a resolution of 320 x 256 pixels. The measurement was carried out at the opposite side of the specimen and the surface was prepared with a black matt lacquer for a high emissivity. The emissivity was determined from the ratio of measured temperature with thermocouples to measured temperature of the IR camera to $\varepsilon = 0.9$.

2.3. Marciniak test

The Marciniak test according to DIN EN 12004-2 [15] is used for the determination of forming limit curves (FLC). The general test setup is shown in Figure 1. To provide a frictionless and planar forming region as in the tensile test, the flat punch was modified by a blind-hole drilling with a diameter of d = 50 mm (red marking). During the test procedure, the punch deep draws the blank with a speed of 1 mm·s^{-1} up to failure. The strains on the sheet surface are recorded with the optical measuring system ARAMIS. The Marciniak tests were carried out on the ERICHSEN universal sheet testing machine for different specimen geometries which are shown in Figure 1. The length of the cut-out is abbreviated L, R the radius and B the remaining width of the blank. By varying B, different stress states can be realized from narrow specimens ($B = 30\ mm$) with a stress state of $\eta = 0.33$ (approximately uniaxial) to wider specimen ($B = 90\ mm$) with $\eta = 0.4$ (approximately plane strain) [16]. In addition to the ARAMIS measuring system, the FLIR A35 IR camera was integrated into the test setup. Since both stationary measuring systems take two measurements on the same side of the blank, a black matt background with a white stochastic lacquer pattern was applied, taking the emission and reflexion into account. In addition, a blue light was used for the measurement to reduce the effects of radiation. The other settings were similar to the tensile test.

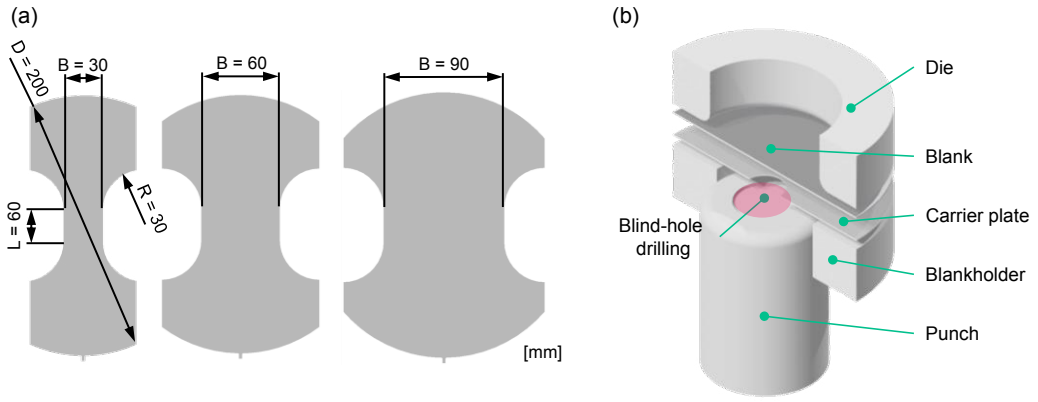

Fig. 1. Specimen geometries (a) and general test setup (b) according to DIN EN 12004-2 [15] used for Marciniak tests.

3. Numerical approach and model

The chosen method to calculate the dependency of the effective plastic strain on the Taylor-Quinney-coefficient is based on the fundamental balance of energy for solid bodies. Preceding studies have shown that radiation and convection with the surrounding ambient can be neglected for the considered test cases. Therefore solely the heat conduction is taken into account.

$$\frac{\partial T(x,y,t)}{\partial t}\rho c_v = \lambda \cdot div\left(grad\left(T(x,y,t_i)\right)\right) + \dot{q} \tag{3.1}$$

In this equation $T(x,y,t_i)$ represents the temperature field, measured at the discrete times t_i and is taken from the measurements. The density ρ, the heat capacity c_v and the heat conductivity λ are material parameters of the steel. The volumetric term q comprises heat sources. In this case, it contains the heat generated by plastic work and is defined as described above:

$$\dot{q} = \beta_{diff}\bar{\sigma}(\boldsymbol{\sigma})\dot{\varphi}_{v,M} \tag{3.2}$$

In order to circumvent the difficulty to determine the prevailing state of stress $\boldsymbol{\sigma}$ in the sheet material during testing, the yield function is used to describe the equivalent stress by means of the yield stress, which is a function of the effective plastic strain. This is accessible by evaluating the measured deformation field and the flow curve described with equation (2.3). It is assumed that the elastic strains are negligible.

$$\dot{q} = \beta_{diff}k_f(\varphi_{v,M})\dot{\varphi}_{v,M} \tag{3.3}$$

Instead of directly evaluating the given differential equation (3.1) a discrete approach is chosen based on the finite volume method. Therefore, the mid region is subdivided in five volumes, which share a cross section as shown in Figure 2. The heat balance is set up for the volume in the center V_c by integrating over the volume.

$$\int_{V_c}\frac{\partial T(x,y,t)}{\partial t}\rho c_v\, dv = \int_{V_c}\left\{\lambda \cdot div\left(grad\left(T(x,y,t)\right)\right) + \dot{q}\right\} dV \tag{3.4}$$

The volume integral of the divergence term is transformed into a surface integral.

$$\int_{V_c}\frac{\partial T(x,y,t)}{\partial t}\rho c_v\, dv = \lambda\int_{A}\left\{grad\left(T(x,y,t)\right)\right\}\circ \boldsymbol{n} da + \int_{V_c}\beta\left(\varphi_{v,M}\right)k_f\left(\varphi_{v,M}(x,y,t)\right)\dot{\varphi}_{v,M}(x,y,z)\, dV \tag{3.5}$$

In order to evaluate the given integrals, it is assumed that the temperature as well as plastic strains are averaged over the volume ($T_c(t)$). An average temperature for the considered volume is computed for each given frame.

$$V_c\frac{\partial T_c(t)}{\partial t}\rho c_v = \lambda\int_{A}\left\{grad\left(T(x,y,t)\right)\right\}\circ \boldsymbol{n} da + V_c\beta\left(\varphi_{v,M,c}\right)k_f\left(\varphi_{v,M,c}\right)\dot{\varphi}_{v,M,c} \tag{3.6}$$

The heat conduction term is described with the help of a finite difference quotient.

$$\lambda\int_{A}\left\{grad\left(T(x,y,t)\right)\right\}\circ \boldsymbol{n} da = \sum_{i=1}^{4}\frac{\lambda A_i(T_c - T_i)}{l} \tag{3.7}$$

Here l is the length between the midpoint of the volume in the center (V_c) and the respective midpoint of the neighboring volume. With help of these manipulations the differential Taylor-Quinney-coefficient can be determined using the measured data and taking into account heat conductivity.

$$\beta_{diff}\left(\varphi_{v,M,c}(t_i)\right) = \left(V\frac{\partial T_c(t_i)}{\partial t}\rho c_v - \sum_{i=1}^{4}\frac{\lambda A_i(T_c - T_i)}{l}\right)\cdot\frac{1}{k_f\left(\varphi_{v,M,c}\right)\dot{\varphi}_{v,M,c}V_c} \tag{3.8}$$

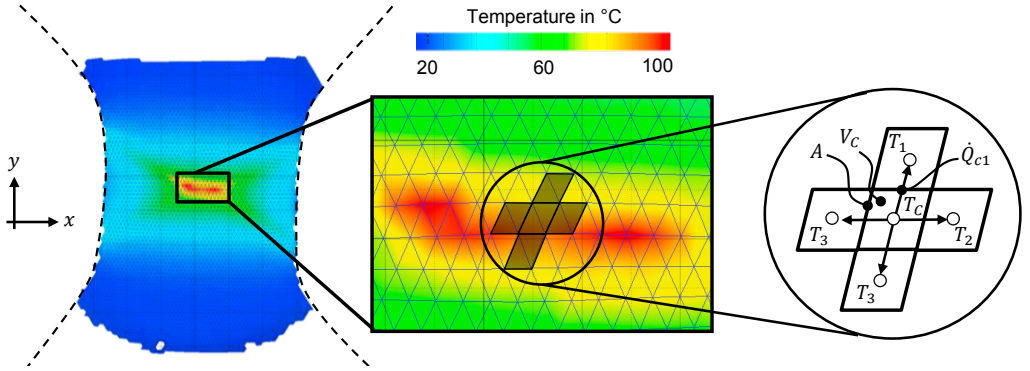

Fig. 2. Evaluation of the temperature field in the region of interest for the Marciniak test.

4. Results and discussion

4.1. Tensile test

In the tensile test, it can be observed that the local temperatures rise against local strains. The ductility and work hardening behavior, and therefore the plastic work of the HCT980X are decisive for the fraction of plastic work converted into heat. During the uniform elongation, the temperature distribution is consistent to the strains that arise. Thus, a homogeneous temperature and strain distribution over the gauge length can be detected. With the beginning of the necking, the maximum strains and temperatures gradually concentrate on the necking zone during forming. Thereby the local strain rate $\dot{\varphi}_{v,M}$ deviate from the process strain rate, here called global strain rate $\dot{\varphi}$, which has been defined for the experimental procedure. Before cracking, a strain localisation takes place where the temperature increases significantly, exceeding the temperature in other regions of the specimen.

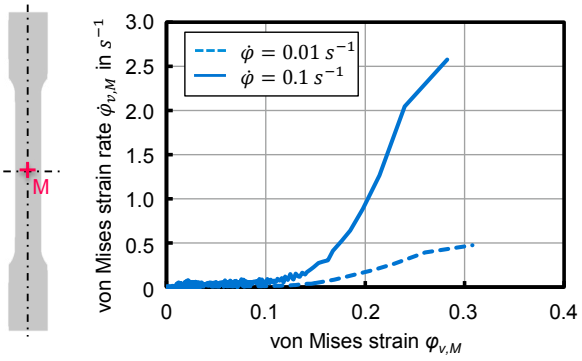

Fig. 3. Local strain rate vs. strain from tensile test at global strain rates of $\dot{\varphi} = 0{,}01\ s^{-1}$ and $\dot{\varphi} = 0{,}1\ s^{-1}$.

In order to evaluate the dependence of the Taylor-Quinney coefficient on the local strain rate, the maximum values of the point of maximum temperature (M) have been calculated using data from DIC. Figure 3 shows results of the local strain rate in the middle of the tensile specimen for two different global strain rates. In general, higher global strain rates lead to higher maximum local values. The local strain rate $\dot{\varphi}_{v,M}$ rises with increasing strain $\varphi_{v,M}$. However,

a significant increase can be observed after the end of the uniform elongation at $\varphi_{v,M} \approx 0.11$ for $\dot{\varphi} = 0.01\ s^{-1}$ and $\varphi_{v,M} \approx 0.15$ for $\dot{\varphi} = 0.1\ s^{-1}$. These values were determined by means of the flow curve. During the necking process, the distance between the two curves increases gradually. Before cracking, the maximum local strain rate of $\dot{\varphi} = 0.1\ s^{-1}$ is five times as high as with $\dot{\varphi} = 0.01\ s^{-1}$.

In addition, the differential Taylor-Quinney coefficient β_{diff} was calculated on the basis of equation (3.7). The aim is to obtain an estimation of the influence of local strain and strain rate. In Figure 4, the curves of β_{diff} as a function of strain are shown for different global strain rates. In order to illustrate the influence of heat conduction, each diagram contains two curves. Dashed lines are used for a Taylor-Quinney coefficient under adiabatic conditions and solid lines for a Taylor-Quinney coefficient including heat conduction.

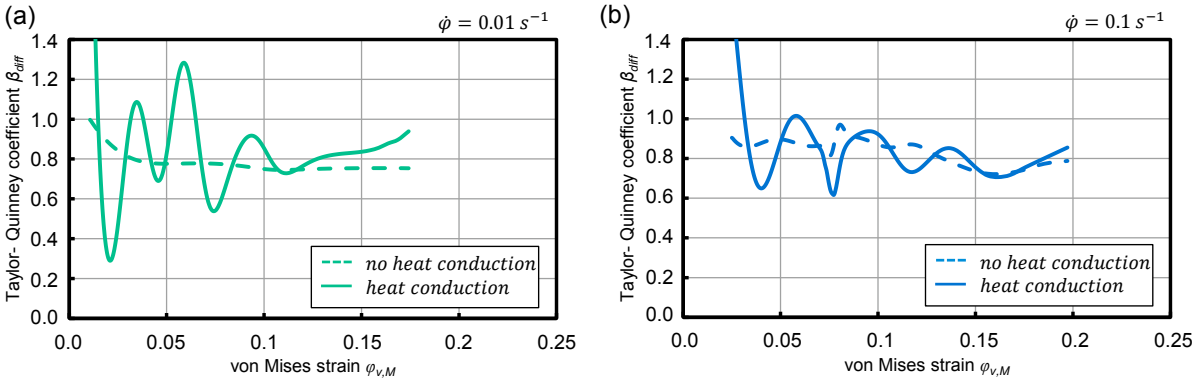

Fig. 4. Taylor-Quinney coefficient vs. strain from tensile test at different global strain rates of $\dot{\varphi} = 0{,}01\ s^{-1}$ (a) and $\dot{\varphi} = 0{,}1\ s^{-1}$ (b).

It can be shown that β_{diff} is variable and depends on the distributed plastic strain and the strain rate. Plastic strains less than $\varphi_{v,M} = 0.02$ could not be calculated properly because in this area strain as well as temperature changes were negligible small. Without heat transfer effects, the Taylor-Quinney coefficient has approximately a constant value of 0.8 for $\dot{\varphi} = 0.01\ s^{-1}$. At the higher strain rate (Fig.4 b), the values fluctuate stronger. Heat conduction has a major influence on β_{diff} for both global strain rates. At $\dot{\varphi} = 0.01\ s^{-1}$ very large amplitudes and an alternating dependency on the plastic strain are shown at the beginning of the forming process. Even small fluctuations of the computed heat flux have a high impact on the Taylor-Quinney coefficient. Nevertheless, the value of β_{diff} fluctuates around the adiabatic value. For $\dot{\varphi} = 0.1\ s^{-1}$, the amplitudes decrease because there is less time for heat exchange between adjacent volumes. With an increase of strain, the effect of heat conduction increases for both global strain rates. At lower global strain rates more heat is conducted from the center to the adjacent volumes due to slower testing procedure. After the beginning of necking at $\varphi_{v,M} \approx 0.11$ for (Fig.4a) and $\varphi_{v,M} \approx 0.15$ for (Fig.4b), the curves rise linearly with increasing strains. According to Figure 3, this behaviour can be determined from the significantly higher local strain rates. The results show that the assumption of a constant Taylor-Quinney coefficient in the tensile test seems to be invalid for the investigated material.

4.2. Marciniak test

By means of the Marciniak test, the observations in the tensile tests can be confirmed and even extended. The local strain rates obtained by the various specimen geometries are lower than those measured in the tensile test. In Figure 5, it is shown that there are minor variances between the different specimen geometries.

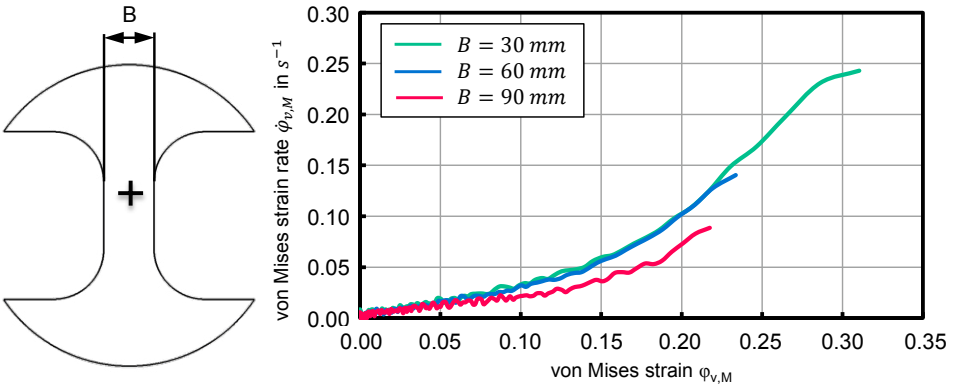

Fig. 5. Local strain rate vs. strain for different stress states from Marciniak test with a punch speed of $v = 1\ mm \cdot s^{-1}$.

Higher local strain rates are obtained with increasing strains. The different specimen geometries lead to a varying forming behavior. If the specimen cracks later (see Fig.5 $B = 30\ mm$), higher maximum strain rates are obtained. In comparison to the tensile test, the course of the strain rate has an influence on the Taylor-Quinney coefficient, especially on the heat conduction, which is illustrated in Figure 6.

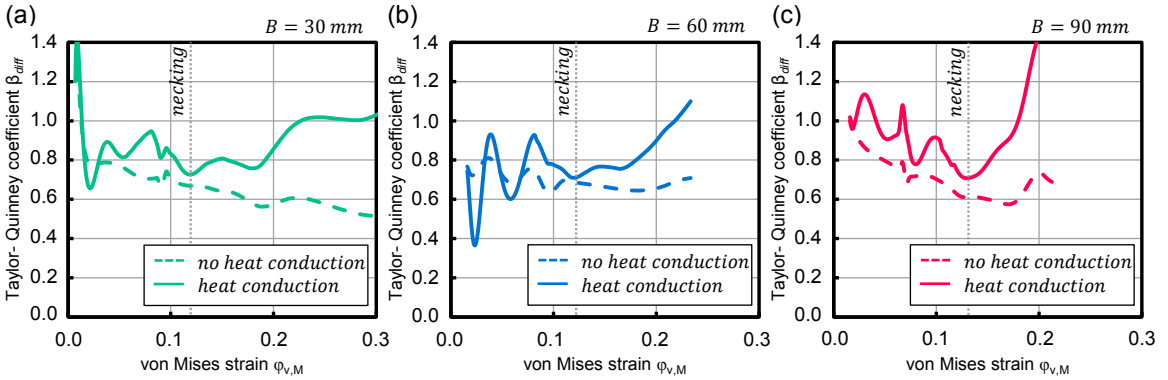

Fig. 6. Taylor-Quinney coefficient vs. strain for different stress states (a-c) from Marciniak test with a punch speed of $v = 1\ mm \cdot s^{-1}$.

In general, the values of β_{diff} without heat transfer effects are lower than in the tensile test. Starting with a Taylor-Quinney coefficient of $\beta_{diff} = 0.8$, the curves decrease to a value of 0.6. Taking the heat conduction into account β_{diff} is alternating up to the beginning of necking, which can be localized with the rapid rise of the strain rate curves in Figure 5. During necking, all curves rise linearly with increasing strains. Compared to the tensile test the heat conduction seems to have a greater influence. With an increasing specimen width B (see Fig.1), the Taylor-Quinney coefficient rises more strongly because more material is in contact with the punch, which leads to a higher heat flow through the region of interest. It seems that the stress state has only a minor influence on the Taylor-Quinney coefficient.

5. Conclusion

In this paper an experimental and numerical approach to determine the influence of local strain, strain rate and stress state on the Taylor-Quinney coefficient in two different test setting have been presented. In this respect, an industrially relevant high-strength steel HCT980X was investigated. The experimental setup was capable of obtaining repeatable measurements of the local mechanical and thermal field quantities. It has been shown that for HCT980X, the Taylor-Quinney coefficient is variable over the course of the effective plastic strain. The global strain rate and in this context the local strain rate is an influencing factor for the heat conductivity. Higher strain rates lead to a shorter

process times, so less heat is dissipated due to heat flux. After necking, a large amount of heat is generated due to large plastic deformations. Therefore, the Taylor-Quinney coefficient rises linearly with increasing strains. The stress state seems to have a minor influence on β_{diff}. The different specimen geometries which are in contact with the punch are decisive for the Taylor-Quinney coefficient. Therefore, the remaining width B of the specimen leads to different thermal conditions, causing different heat conduction rates.

Acknowledgements

The IGF-Project "Extension of heat release rate modeling for steels"of the European Research Association for Sheet Metal Working (EFB e.V.) was funded by the Federal Ministry of Economics and Energy (BMWi) under the funding number 19245N of the German Federation of Industrial Research Associations (AiF) on the basis of a decision by the German Bundestag. The authors would like to thank for this financial support.

References

[1] W. S. Farren; G. I. Taylor. The Heat Developed during Plastic Extension of Metals. Proc. R. Soc. Lond. A 1925 107 (1925) 422-451.
[2] G. I. Taylor; H. Quinney. The Latent Energy Remaining in a Metal after Cold Working. Proc. R. Soc. Lond. A 1934 143 (1934) 307-326.
[3] R. Zaera; J.A. Rodriguez Martinez; D. Rittel. On the Taylor–Quinney coefficient in dynamically phase transforming materials. Application to 304 stainless steel, International Journal of Plasticity (2013) 185 – 201.
[4] D. Macdougall. Determination of the plastic work converted to heat using radiometry, Experimental Mechanics 40, (2000) 298-306.
[5] J. J. Mason; A. J. Rosakis; G. Ravichandran. On the strain and strain rate dependence of the fraction of plastic work converted to heat: an experimental study using high speed infrared detectors and the Kolsky bar. Mechanics of Materials 17 (1994) 135-145.
[6] P. R. Dixon; D. J. Parry. Thermal softening effects in type 224 carbon steel. Colloque C3, suppl. au Journal de Physique III, Vol. 1 (1991) 85-92.
[7] P. Knysh; Y.P. Korkolis. Determination of the fraction of plastic work converted into heat in metals, Mechanics of Materials 86 (2015) 71-80.
[8] B. Fekete; A. Szekeres. Investigation on partition of plastic work converted to heat during plastic deformation for reactor steels based on inverse experimental-computational method, European Journal of Mechanics A/Solids 53 (2015) 175-186.
[9] D. Rittel, L.H. Zhang, S. Osovski. The dependence of the Taylor–Quinney coefficient on the dynamic loading mode, Journal of the Mechanics and Physics of Solids, Vol. 107 (2017) 96-114.
[10] B.-A. Behrens; C. Bonk; M. Vucetic; A. Bouguecha. An Experimental-Nurmerical Method to Determine the Plastic Work Converted into Heat Applied on AHSS. Advanced Materials Research, Vol. 1140 (2016) 51-58.
[11] B.-A. Behrens; T. Götze. Temperature-dependent anisotropic material modeling of the sheet metal component within the polymer injection forming process, Production Engineering (2013) 91-99.
[12] H. W.,. Swift. Plastic instability under plane stress. Journal of the Mechanics and Physics of Solids, 1 (1) (1952) 1–18
[13] E. Voce. The relationship between stress and strain for homogeneous deformation. Journal of the Institute of Metals, 74 (1948) 537–562.
[14] DIN EN ISO 6892-1. Metallische Werkstoffe – Zugversuch – Teil 1: Prüfverfahren bei Raumtemperatur. (2009).
[15] DIN EN ISO 12004-2. Metallische Werkstoffe – Bleche und Bänder - Bestimmung der Grenzformänderungskurve – Teil 2: Bestimmung von Grenzformänderungskurven im Labor. (2009).
[16] B.-A. Behrens; A. Bouguecha; M. Vucetic; I. Peshekhodov. Characterisation of the quasi-static flow and fracture behaviour of dual-phase steel sheets in a wide range of plane stress states, Archives of Civil and Mechanical Engineering (2012) 397 – 406.